Jurnal Kejuruteraan 37(7) 2025: 3301-3312
https://doi.org/10.17576/jkukm-2025-37(7)-15

Enhanced Flywheel Energy Storage Using Speed-Controlled Dual Drives and Star-Delta Switching

Ramizi Mohamed[a*], Mohd Shamsul Ali[b], Muhammad Ammirrul Atiqi Mohd Zainuri[a], Muhamad Zalani Daud[b], & Mahidur R. Sarker[c,d]

[a]*Department of Electric, Electronics and System Engineering, Faculty of Engineering and Built Environment, Universiti Kebangsaan Malaysia, Bangi 43600, Malaysia*

[b]*Renewable Energy and Power Research Interest Group, Faculty of Ocean Engineering Technology, Universiti Malaysia Terengganu, 21030 Kuala Nerus Terengganu, Malaysia*

[c]*Institute of Visual Informatics, Universiti Kebangsaan Malaysia, Bangi 43600, Selangor, Malaysia*

[d]*Industrial Engineering and Automotive, Nebrija University, Campus de la Dehesa de la Villa, Calle Pirineos, 55, 28040 Madrid, Spain*

[*]*Corresponding author: ramizi@ukm.edu.my*

Received 12 March 2025, Received in revised form 22 June 2025
Accepted 22 July 2025, Available online 30 October 2025

ABSTRACT

Flywheel Energy Storage System (FESS) plays a crucial role in enhancing power quality in renewable energy systems, particularly in isolated micro-grids. However, challenges such as power supply consistency, lack of inertia from power electronics converters, and high starting currents in induction motors necessitate further improvements. This study aims to improve FESS performance by introducing a speed-controlled double star-delta configuration with low-power double drives for flywheel motor-generator (FMG) synchronization. The proposed methodology involves developing a prototype system with a double three-phase star-delta configuration, employing a low-power induction motor for FMG speed synchronization. A Programmable Logic Controller (PLC) with a Human-Machine Interface (HMI) is integrated for control and monitoring, utilizing a PID-based closed-loop control system. The system is tested in a laboratory environment with various flywheel weights to evaluate its performance. Experimental results demonstrate that the double star-delta configuration effectively synchronizes FMG speed while reducing power consumption. The star connection provides stable frequency and lower starting torque, while the delta connection offers higher torque, ensuring efficient flywheel acceleration. The experimental results showed that this system of hybrid star-delta with a double low-power three-phase induction motor can drive a high-inertia flywheel of up to 100 kg and synchronise the speed of the system to the nominal speed of the generator up to 1500 rpm. The proposed system minimizes energy losses, optimizes starting conditions, and reduces overall development and maintenance costs. These findings indicate that the integration of a low-power double motor and a controlled switching mechanism significantly enhances FESS efficiency, making it a viable solution for sustainable energy applications.

Keywords: Flywheel Energy Storage System; Flywheel motor generator system synchronisation; power consumption reduction; voltage and frequency stability.

INTRODUCTION

An established technology that has a noticeable effect on the quality of the power generation system is the flywheel energy storage system (FESS). The FESS can increase the percentage of power quality of the renewable energy generators in isolated micro-grids. The contribution of the FESS in an isolated micro-grid that combines a diesel generator, wind turbine and hydro turbine power station is in the improvement of frequency deviations and regulation (Garcia-Pereira et al. 2022). Flywheel-battery hybrid system has the advantage of providing grid frequency regulation support with combined two type of energy storage (Cao et al. 2023). FESS provides a new solution for handling high-frequency power fluctuation of renewable energy generation in practical application scenarios for power grid control (Mahrouch et al. 2024). An integrated system hybrid between battery and flywheel can elongate the operational time of the battery in comparison to a stand-alone battery (Mouratidis, Schubler, and Rinderknecht 2019). In FESS, the high speed of the motor is the main energy conversion factor which can change the amount of energy stored during charging and discharging electrical power (Zhou et al. 2020).

However, the problem with the microgrid is the storage system and how they coordinate with each other to guarantee the supply of power consistently to the loads in grid-connected modes. In some microgrid applications, it is composed of double FESS, where each one of them can be connected either to a photovoltaic (PV) array or to a wind turbine purposely to absorb the excess power generated and restitution when load changes occur (Nemsi et al. 2018). The second issue is that renewable energy sources are typically connected to the power grid through power electronics converters which do not naturally supply inertia like synchronous generators (ALI et al. 2021). Utilising FESS to offer virtual inertia and frequency support is one way to address the lack of inertia problem (Yu, Fang, and Tang 2018). An energy storage system's goal is to efficiently restore electricity by reducing the outage time because it has flexible charging and discharging capabilities. Flywheel energy storage was therefore taken into consideration as a means of restoring the power system (Xie et al. 2023). Problems like power variations in distribution or intermittent renewable energy can be solved with the correct energy storage technology. To deliver energy and power, a hybrid energy storage system consists of two or more storage devices with integrated electrical charge and discharge characteristics. Energy density and power density are the two primary supporting features of energy storage systems. To facilitate the provision of intermittent energy, flywheel energy storage (FES) and battery energy storage (BES) technologies are coupled to form the major component of a hybrid energy storage system (ALI 2021). However, High-speed operation and frequent load changes can cause heat buildup, particularly in the motor drives and switching devices.

An energy-powered hybrid energy storage system with a lithium battery and flywheel can be used to lower the cost of energy storage and increase its output performance. Lithium batteries and flywheels can be coupled to high-frequency and low-frequency components, which together comprise the hybrid energy storage system's total cut-off frequency. A hybrid energy storage system's capacity optimisation configuration model is configured to limit the maximum ramp rate of lithium battery charge/discharge power, maximise flywheel power, and minimise flywheel capacity (Zhao et al. 2023). In superconducting flywheel energy storage, the density is mostly determined by their design, which applies compressive stress on the uppermost layer and layers of uneven thickness (Prasanthi et al. 2021). An EV charging station with an uneven load curve can use the peak shaving control for load balancing using the microgrid and FESS. Applying FESS for peak shaving management demonstrates that an unbalanced load ranging from 7 to 230 kW may be resolved (Bekiroglu and Esmer 2023). A pulsed power supply system combined with FESS and a modular multilevel cascade converter is used for power compensation when performing rapid excitation of highly inductive and pulsed heavy loads. This integrated system consists of an induction motor with a flywheel to store kinetic energy and capacitors to cause a self-excitation factor in an induction motor that is parallel connected, and it works as an induction generator (Murayama et al. 2018).

In industry, three-phase induction motors are most commonly used in various electrical drives (Anjitha et al. 2017). In the FESS application, an induction motor was chosen to drive the flywheel and generator, as developed in (Huang and Chen 2017), (Ferreira et al. 2020). Star-delta is purposely used to reduce starting voltage and current in the industrial motor. A Gate-Turn-Off (GTO) switch has been used to replace the relay contact switch and a thyristor star-delta switch is applied as a soft starter that contributes to saving energy when using a delta connection. In industrial environments, variable-speed drives and electronic soft starts are frequently used to enable star-delta starting from a low voltage supply without the need for a sizable induction motor with a high-power output of more than 4 kW (Premkumar and Sowmya 2017). The star-delta starter is a low-cost electromechanical starter that can reduce starting voltage. Voltage starting with star configuration is 230V across each winding, meanwhile with delta configuration is 400V across each winding. Changing from star to delta has the disadvantage of decreasing starting torque by about 67%, for example from

1038 Nm to 343 Nm. The factor of reducing voltage when starting with star configuration is about triple by measuring voltage for star configuration is 219.3V but delta configuration is 380V. The cost of this configuration is lower and can be easily commercialized. In (Saputra, Suryawan, and Sugirianta 2020), a proposed Delstar converter is put forth to reduce the amount of energy used by the system when there is no load operation or a load that is less than 40% of the full load. This converter switches the system from delta mode to star mode. Implementing this method in larger or grid-scale storage systems might present challenges due to limitations in drive and switch performance. In (Dwivedi et al. 2017), the voltage, current, and speed of both mode star and delta operations were visualised using LabVIEW and Arduino to illustrate the star-delta starting operation. Using dual drives and switching mechanisms introduces more components, which can increase the cost, weight, and maintenance requirements of the system.

Three-phase induction motors draw a high current during starting operation in full-load running conditions (Dwivedi et al. 2017). Various methods have been developed to reduce the starting current of the induction motors, such as the implementation of relays and electronic timers. Induction motor operation: if not switched to delta mode within a few seconds, the motor can draw heavy current and burn itself out. For this purpose, an automatic star-delta controlled relay and electronic timer were used to switch the induction motor operation from delta to star configuration. Induction motors are popular and widely used in industry applications due to their low cost, rugged construction, fast pick-up, low maintenance cost, and good efficiency (Itajiba et al. 2021). The start-delta connection used to run induction motors during starting and operation protects against voltage fluctuations and single phasing. Figure 1 shows the sudden increase in stator current when switching modes from star to delta connection. The star-delta switching process can lead to temporary power instability or losses, especially if not timed accurately. Heavy current drawn by the induction motors during starting can damage them. An enhancement of soft starting with a firing angle controlled by the induction motor can overcome the drawback of the star-delta starter. An induction or asynchronous motor is widely used in industry as an industrial drive because it offers a variable-speed version by using variable-frequency drives for controlled-speed applications. The most common type of induction motor used in industry is the squirrel cage motor because it has no brushes and is rugged (Musa et al. 2024). Traditional methods such as DOL, autotransformers, and fixed star-delta starters can control the high starting current during the starting period only at certain limits. As the induction motor accelerates, the current will begin to drop slowly until the motor achieves 85% synchronous speed. Therefore, the motor load will affect the time taken by the motor to achieve full speed and the duration of the high starting current. The importance of starting time is referred to as the duration of a large current flow during the starting of an induction motor (Bokde et al. 2017). However, The star-delta switching process can lead to temporary power instability or losses, especially if not timed accurately.

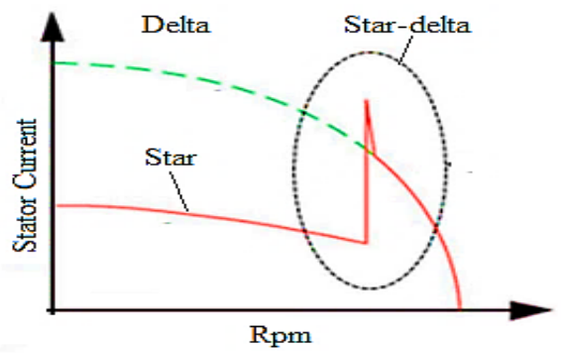

FIGURE 1. Starting current of star-delta switching.

Induction motors commonly convert approximately 50% of all the electricity generated. The star-delta starter is commonly used for starting induction motors and is interfaced with converters used for power saving due to the low power consumption of the star-mode operation, which is almost 1/3rd of delta-mode power consumption (Nuraqilah et al. 2023). When the load is less than 30% of the full load, the motor can swiftly switch to star mode operation to save power. Meanwhile, the delta mode is necessary for full-load operation at the starting condition, which requires high torque to drive a high-inertia flywheel or load. If star mode is used for full-load operation, the drawback is high current will damage the inverter. The switching arrangement of star-delta at a suitable reduced load can improve efficiency and power factor compared to a fixed star-delta configuration. Authors (Usha et al. 2024) implemented a double-star induction motor to drive the flywheel in the FESS. This novel method of the drive system can satisfy the requirements of wind power production systems. In the past, the DC motor was the most popular drive due to its excellent controllability, but nowadays, the three-phase AC motor is the modern, high-performance motor drive system. Induction motors are employed in textile factories, agriculture, and almost all manufacturing industries to drive loads due to their rugged construction and easy operation, but they still have limitations due to their efficiency and power factor. Two possible delta connections that give different results are known as common and preferential. These two delta

connections give rise to a switching current of either small or higher amplitude.

To increase the speed of the induction motors, a multiphase supply needs to be hired. Enhancement of the speed range in the multiphase machine can be achieved by applying a high-voltage inverter or field weakening technique by changing the phase sequences (Ramesh et al. 2018). The speed of the induction motors can be changed by applying various methods, such as poles or voltage-changing methods, but the most efficient method is changing frequency and voltage by hiring a variable frequency drive (VFD). VFD provides efficient operation with speed and torque control according to the load requirements. Besides that, VFD can also lead to the harmonics issue of motor performance (Kusmantoro, Theodora Indriati, and Ristanto 2017). In (Koradiya and Solanki 2019), the fuzzy logic-controlled soft starter for the induction motor in a delta connection is proposed to control the stopping and starting operations with safety or protection added. This configuration not only offered a low starting current but also enough torque to drive the load. Application of an AC drive or VFD to the induction motors can be a more cost-effective approach to the system. Authors in (Soheli and Hasan 2018) proposed Pole Amplitude Modulation (PAM) to create a very low output current for multi-speed and high-horsepower applications. By using a single motor to offer high horsepower, it can be energy-efficient and reduce the cost of the motor. In (Shubham et al. 2016), an inverter was implemented to reduce the star delta starter voltage for a 3-phase motor. This proposed method is suitable for variable-frequency drives and high-power applications. The inverter can provide proper frequency, current, voltage, and starting torque. To overcome the disadvantage of conventional types of contactors, authors in (Ibrahim Shahl 2018) proposed static switching by using a Raspberry Pi controller for a star-delta starter. In (Pindoriya et al. 2018), the simulation analysis of the induction motor starting model to improve electrical power quality is presented. This analysis focuses most on the voltage sags and harmonics issues of the motor's starting operation. Authors in (ALI et al. 2021) used a speed controller in the FESS application to control the speed of the three-phase motor by applying a three-phase inverter. Thus, the most widely used electrical machines and devices for achieving higher efficiency for speed control and power consumption reduction in industrial or FESS applications are three-phase inverters and three-phase induction motors, either with a star or delta connection. However, coordinating speed control between dual drives and managing star-delta transitions requires a sophisticated control algorithm, increasing design and implementation complexity.

MATERIALS AND METHODS

For analysis of the difference in amplitude of frequency for the double star and delta connection, a prototype of the FMG speed synchronisation was assembled in the laboratory with a double three-phase controlled double star-delta and a low-power double three-phase induction motor. The induction motor-type squirrel cage was used as a standard sample for lab scale analysis with a nominal rating power of 0.3 kW, 400-Y/380-Δ V, 4 poles, 2800 rpm, 0.84 A, and a power factor of 0.84. The synchronous generator is used with a nominal power rating of 0.3kW, 400V, 0.7A, 1500rpm, and 50Hz. The circuit diagram of the overall drive system is shown in Figure 2.

There are two frequency inverters applied to the system to control the speed and torque of the system. As shown in the diagram Figure 2, a single-phase power supply of 240V and 50Hz is used to power the inverter. These two inverters generally invert the power supply from a single-phase to a double-three-phase supply. This double three-phase supply is used to power the induction motors, which are in M1 and M2 connections. These three-phase inverters consist of a full-wave rectifier, filtering, and a three-phase full-bridge inverter circuit. The frequency of the inverter can be changed depending on the requirements of the system.

Regarding the controller, the PLC-Programmable Logic Controller was chosen to control the overall system, which offers easy communication through serial interfacing and simple implementation. The PLC model Siemen S7-1500 with Human Machine Interface (HMI) was adopted in the system. This controller used to control the sequential of the star-delta by controlling the inverter. HMI displays the parameters of the FMG synchronization. This speed synchronisation is applied when PID closed loop control is programmed in the PLC. The speed sensor used to be a device that gave a signal to the PLC. This sensor is located at the FMG shaft. At the same time, PLC also controlled the ramp of the current frequency of the inverter. Ensuring precise synchronization between the flywheel motor and generator during transitions can be difficult, leading to possible torque ripples or power losses.

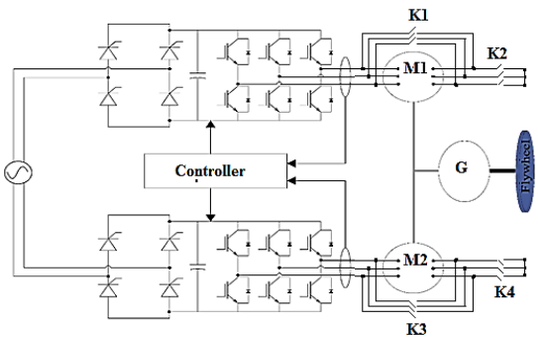

FIGURE 2. Circuit diagram of the proposed drive system.

A mechanical topology of the FMG connected each other is as shown in Figure 3. This studied topology is a lab-scale specification. These FMGs are directly coupled using a rubber coupler. The servo machine acts as a simulated flywheel, which can be regulated to different inertial. Three-phase induction (TIM) M1 and M2 in double star and double delta connections are used to drive the flywheel and synchronous generator (SG). The flywheel motor-generator system stores kinetic energy using a rotating mass (flywheel) connected to a motor-generator unit. A flywheel is a high-inertia rotating mass, usually made of steel or composite material, mounted on a shaft. Motor-Generator (MG) Unit is a bidirectional machine acting as a motor during charging and a generator during discharging. Coupling is a mechanical coupling (rigid or flexible) that connects the MG shaft to the flywheel. It ensures torque transfer and absorbs minor misalignments, and bearings are precision ball or magnetic bearings that support the flywheel shaft, enabling smooth and low-friction rotation. However, there are a few losses flywheel motor-generator mechanical connection, for example, bearing friction losses in terms of friction in ball or magnetic bearings supporting the flywheel shaft. Air drag losses, which are caused by aerodynamic drag as the flywheel spins (reduced in vacuum enclosures). Coupling losses, which is misalignment or slight slip in flexible coupling, lead to small torque loss.

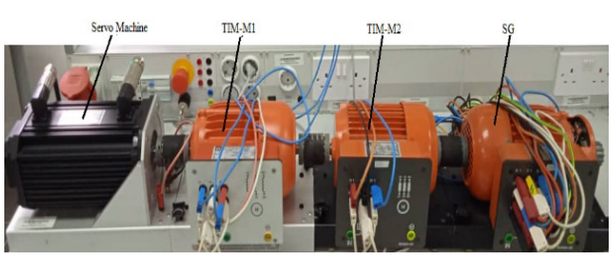

FIGURE 3. Mechanical connection arrangement.

Figure 4 shows configuration of controller and monitoring system for the speed synchronization of FMG which HMI and frequency inverter connected to the PLC. The power supply 24 Vdc/3 A used to power the PLC. HMI displays the figure of FMG with parameter setting and display. The synchronous speed of the FMG can be set at HMI.

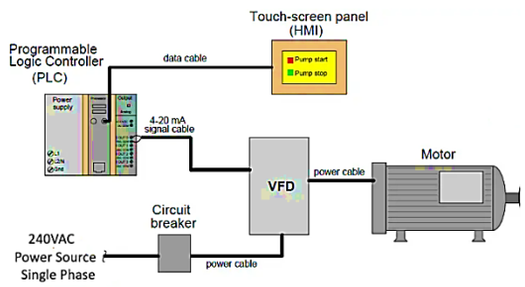

FIGURE 4. Configuration of controller and monitoring system.

The system is analysed using the Simulink model for Star-delta FMG, which is displayed in Figure 5. It is possible to analyse the impact of flywheels with varying sizes and weights using this testing circuit. It is also possible to measure the motor and generator's synchronisation from this testing circuit. The stator current, torque, speed, input voltage, and output voltage of the motor and generator are all being measured. A scope is used to plot the graph, and a multimeter is used to display the RMS value for all measurements. The three-phase supply relay parameter can be adjusted to match the motor specification, and the voltage supply can be adjusted accordingly.

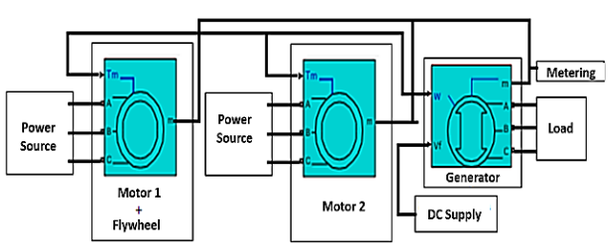

FIGURE 5. Simulink model for Star-delta FMG.

The flow method of the PLC-controlled FMG speed synchronisation is depicted in Figure 6. The speed sensor measures the process variable's (PV) real value and sends it to the PLC, acting as a measuring element in the system. The set point (SP) and the measured value are then automatically compared by the PLC. The PLC determines a signal that represents the required value of the manipulated variable based on the deviation or error count. The FMG speed is synchronised and maintained at the desired value by a continuous process.

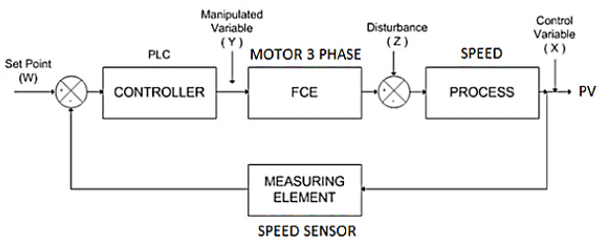

FIGURE 6. FMG speed synchronous flow process.

Figure 7 shows how the speed-synchronous FMG was installed. This installation consists of three areas: field, block panel, and panel. The speed sensor located in the field is connected to a power supply of 24 VDC at the block panel. The signal pin of the speed sensor is connected to the input port of the PLC. The output of the PLC is then connected to the inverter port selection to control the frequency. The output is three-phase from the inverter UVW connected to the TIM.

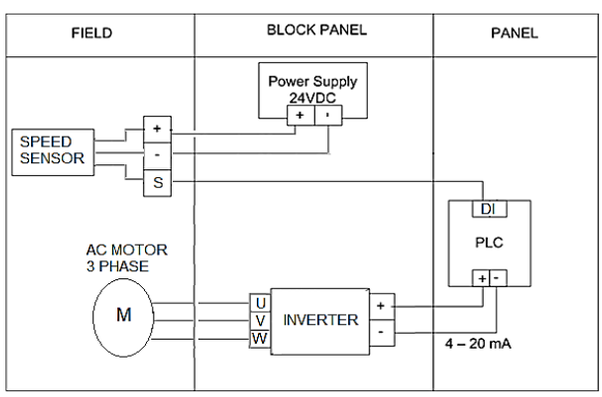

FIGURE 7. Speed/Rpm looping circuit diagram.

The method is a closed-loop or on-line tuning method. Also known as quarter-decay ratio response by ultimate gain. For this tuning method, only a proportional controller is used in the closed-loop system. It consists of two steps: the determination of the dynamic characteristics or personality of the control loop and the estimation of the controller tuning parameters that produce the desired response for the dynamic characteristics determined in the first step. Table 1 shows a guideline for setting the proportional integral derivative (PID) parameters tuned using the closed-loop Ziegler-Nichols method for quarter decay ratio.

MATHEMATICAL MODEL AND EQUATIONS

The inertia of the flywheel is calculated by using the formula:

$$I = \frac{1}{2} m^{2} \tag{1}$$

where I is Inertia, ½ is constant for solid cylinder flywheel, m is the mass of flywheel, r is the radius of flywheel (Bouras et al. 2017).

When star-delta applied to reduce the starting current of the motor, 1/3 of the peak current compared to a direct starting. At the same time, voltage in each phase of the winding is $V_I / \sqrt{3}$. The equation for the winding when connected in star connection can be written

$$I_{PS} = \frac{V_L}{Z\sqrt{3}} \leftrightarrow I_{LS} = \frac{V_L}{Z\sqrt{3}} \tag{2}$$

Where:
I_{PS} is equal to I_{LS}
I_{PS} is winding current per phase
I_{LS} is supply line current
Z is impedance per phase winding
V_L is supply line voltage

When delta connection, the supply line cureent (I_{LSD}) is equal to root three times of the current per phase (I_{PD}) and the winding current per phase is V_L/Z. The equation for the winding when connected in delta connection can be written:

$$I_{LD} = \sqrt{3} I_{PD} = \sqrt{3} \frac{V_L}{Z} \tag{3}$$

When comparing equations

$$\frac{I_{LD}}{I_{LS}} = \frac{\frac{\sqrt{3} V_L}{Z}}{\frac{V_L}{Z\sqrt{3}}} = 3 \tag{4}$$

Therefore, the starting current in case of direct starting delta is three times current of starting delta as calculated in comparing equations (Bekiroglu and Esmer 2023).

The detail Simulink model for Synchronous Generator as shown in figure 4 is used to generate voltage. This model is referring to mathematical model equation:

$$v = [R]*i + dphi/dt + [W]*phi \quad (5)$$

$$phi = [L]*I \quad (6)$$

Where:

R is diagonal matrix (nState, nState) of winding resistances in d q axis

L is matrix (nState, nState) of winding self and mutual inductances in d q axis

W is matrix (nState, nState) depending on rotor speed *wr*, all zero except *W* (1, 2) = *wr*, *W* (2, 1) = -*wr*

v is voltage vector = [*vq* *vd* *vfd* *vkd* *vkq1 (vkq2)*],

phi is flux linkage vector = [*phiq* *phid* *phifd* *phikd* *phikq1 (phikq2)*], (state variable)

i is current vector = [*iq* *id* *ifd* *ikd* *ikq1 (ikq2)*],

if RotorType = Salient-Pole, nState = 5
if RotorType = Round, nState = 6

The detail Simulink model for Asynchronous Motor as shown in Figure 4 used to drive generator and flywheel. This model is referring to mathematical model equation:

$$v = [R]*i + dphi/dt + [W]*phi \quad (7)$$

$$phi = [L]*I \quad (8)$$

TABLE 1. Controller parameter tuning using Ziegler Nichols Method (Bokde et al. 2017).

Type	With overshoot		Without overshoot	
	Disturbance	Reference	Disturbance	Reference
P	$K_P = 0.71\frac{1}{K_S}\frac{T_g}{T_u}$	$K_P = 0.71\frac{1}{K_S}\frac{T_g}{T_u}$	$K_P = 0.3\frac{1}{K_S}\frac{T_g}{T_u}$	$K_P = 0.3\frac{1}{K_S}\frac{T_g}{T_u}$
PI	$K_P = 0.71\frac{1}{K_S}\frac{T_g}{T_u}$ $T_N = 2.3T_u$	$K_P = 0.59\frac{1}{K_S}\frac{T_g}{T_u}$ $T_N = T_g$	$K_P = 0.59\frac{1}{K_S}\frac{T_g}{T_u}$ $T_N = 4T_u$	$K_P = 0.34\frac{1}{K_S}\frac{T_g}{T_u}$ $T_N = 1.2T_g$
PID	$K_P = 1.2\frac{1}{K_S}\frac{T_g}{T_u}$ $T_N = 2T_u$ $T_V = 0.42T_u$	$K_P = 0.95\frac{1}{K_S}\frac{T_g}{T_u}$ $T_N = 1.35T_g$ $T_V = 0.47T_u$	$K_P = 0.95\frac{1}{K_S}\frac{T_g}{T_u}$ $T_N = 2.4T_g$ $T_V = 0.42T_u$	$K_P = 0.59\frac{1}{K_S}\frac{T_g}{T_u}$ $T_N = T_g$ $T_V = 0.5T_u$

Where:
R is diagonal matrix (4, 4) of winding resistances in d q axis
L is matrix (4, 4) of winding self and mutual inductances in d q axis
W is matrix (4, 4) depending on rotor speed *wr* and reference frame
v is voltage vector = [*vqs* *vds* *vqr* *vdr*],
phi is flux linkage vector = [*phiqs* *phids* *phiqr* *phidr*], (state variable)
i is current vector = [*iqs* *ids* *iqr* *idr*],

However, in a FESS that uses speed-controlled dual drives, system losses are a critical factor in determining overall efficiency. These losses come from several sources and can be grouped into mechanical, electrical, and control-related losses. There are a few key losses in terms of mechanical losses, electrical losses, control & operational losses.

RESULTS AND DISCUSSION

The graphs in Figure 8 illustrate the relationship between the weight of the flywheel and the speed of the FMG. The flywheel, three-phase induction motor, and synchronous generator operate at synchronous speed because they are

directly coupled without any pulleys or belts. The frequency converter controls the motor speed. From the graph, the time required to ramp up the motor speed depends on the flywheel's weight. This time is proportional to the flywheel's weight, meaning that increasing the weight will result in a longer time for the motor to reach the generator's required or nominal speed.

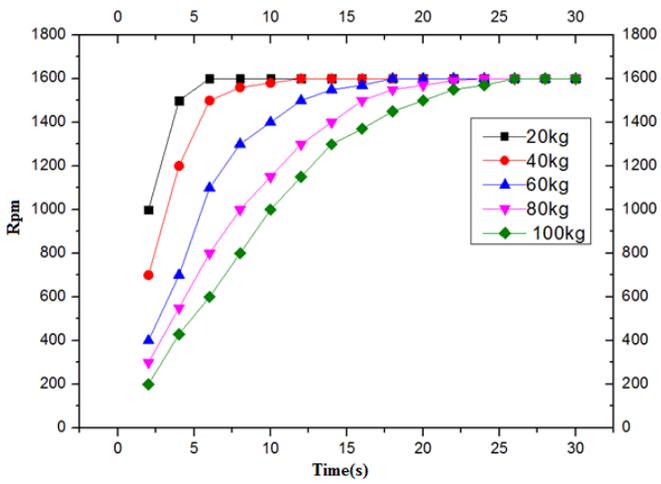

FIGURE 8. Speed of the FMG related to flywheel weight in Star connection.

Figure 9(a) shows the speed of the motor in a star connection, which starts at 0 rpm and takes approximately 18 seconds to reach the desired speed. After 18 seconds, the speed of the motor and generator stabilizes. The synchronous speed of the FMG in this test is 1600 rpm before the system cuts off at 25 seconds. The flywheel is set at a weight of 60 kg with a diameter of 60 cm. After 25 seconds, the motor's power supply is turned off. In this state, the generator continues running, supported by the flywheel. With a 60 cm diameter and a 60 kg flywheel with an inertia of 9 kgm², the generator takes approximately 115 seconds to come to a complete stop. Increasing the flywheel's weight extends the time required for the generator to stop. With a 60 cm diameter and an 80 kg flywheel with an inertia of 14 kgm², the motor stabilizes at 25 seconds, and the generator takes approximately 175 seconds to stop after the power supply is cut off. Figure 9(b) shows that the generator's voltage, which starts at zero volts, increases in proportion to the motor speed. The steady-state voltage of the generator reaches 800 VAC, measured as the phase-to-phase voltage at the generator terminal.

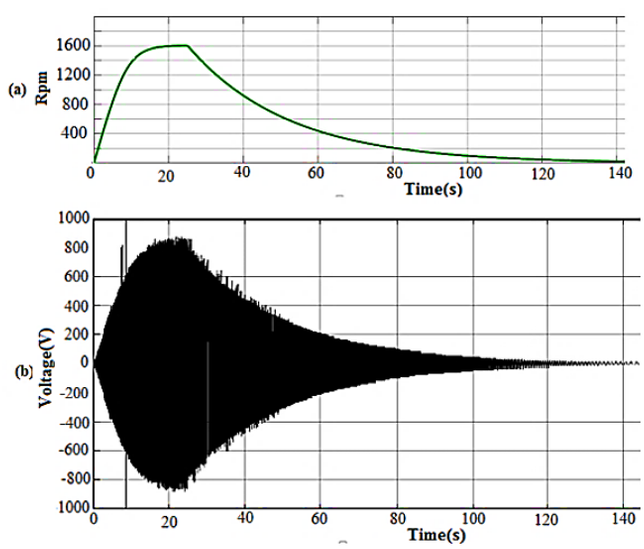

FIGURE 9. Star connection (a) Speed of FMG;
(b) Voltage of SG.

Figure 10(a) shows that in the delta connection, the motor does not start at 0 rpm as it does in the star connection. This indicates that the delta connection provides a high starting torque. In the delta connection, the motor starts at 1400 rpm and takes only 5 seconds to reach the system's desired speed. The synchronous speed of the FMG for the delta connection is also 1600 rpm, controlled by a PID controller linked to the frequency inverter. The flywheel is set at a weight of 60 kg with a diameter of 60 cm. After 25 seconds, the motor's power supply is cut off. In this OFF mode, the generator continues running with support from the flywheel. Like in the star connection, it takes 115 seconds to stop the generator. Therefore, the results show that the type of connection, whether star or delta, does not affect the flywheel's inertia. Figure 10(b) shows that the generator's voltage, which starts at zero volts, increases in proportion to the motor speed. The steady-state voltage of the generator reaches 800 VAC, measured as the phase-to-phase voltage at the generator terminal.

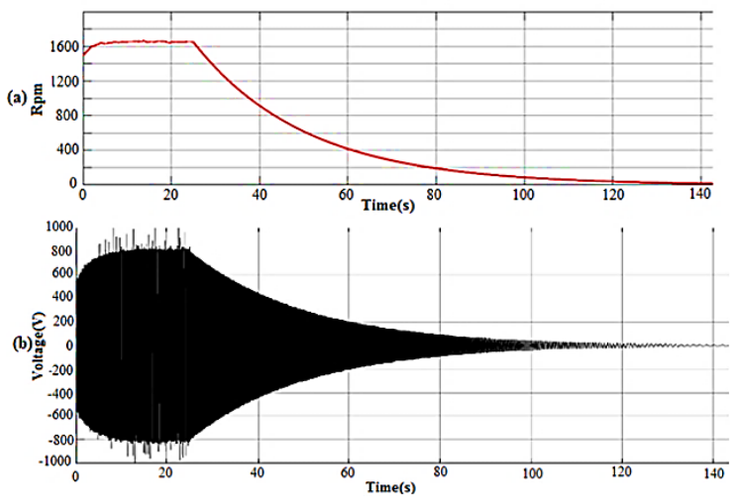

FIGURE 10. Delta connection (a) speed of FMG; (b) Voltage of SG.

The waveforms in Figures 11(a) and 11(b) show that the SG frequency graph pattern is affected by the type of motor connection. The frequency of the SG is approximately 55 Hz. In the delta connection, as shown in Figure 11(a), the frequency is unstable, leading to fluctuations in voltage generation. However, the level of harmonic distortion or ripple is not significantly high. In contrast, the star connection in Figure 11(b) exhibits a smooth and stable frequency from startup to the cutoff period.

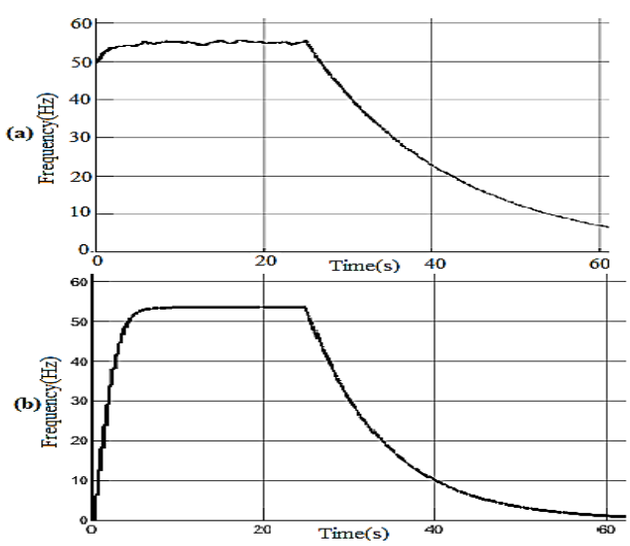

FIGURE 11. Frequency SG (a) Delta connection; (b) Star connection.

Figure 12 illustrates the relationship between torque, current, voltage, and speed in a three-phase induction motor rated at 0.5 kW for both star and delta connections. The power supply for this test is set to 230 VAC and 40 Hz using a frequency inverter. The maximum torque for the delta connection is 1.6 Nm, as shown in Figure 12(a), while the maximum torque for the star connection is only 0.3 Nm, as shown in Figure 12(b). The maximum speed in the delta connection reaches 2400 rpm, whereas in the star connection, it is 2200 rpm.

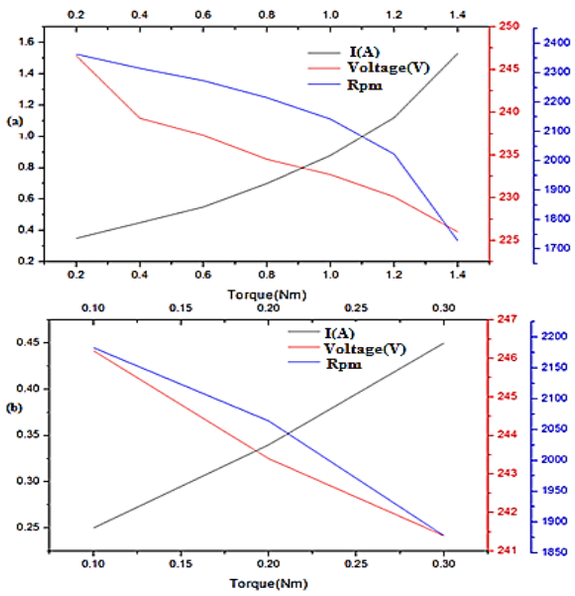

FIGURE 12. Torque, Current, Voltage, Speed of TIM (a) Delta connection; (b) Star connection.

Figure 13 illustrates the mechanical power of the star, delta, double-star, and double-delta configurations. To start a high-weight flywheel, a double-delta configuration is required to drive the flywheel effectively. By using a dual-motor setup with a 0.5 kW three-phase induction motor, the system can generate nearly 3 Nm of mechanical power. After the initial startup, the system can be switched to a double-star configuration, which provides a torque of approximately 0.5 Nm. The motor requires high torque only during the startup phase, whereas for continuous operation, the flywheel requires only a small amount of torque.

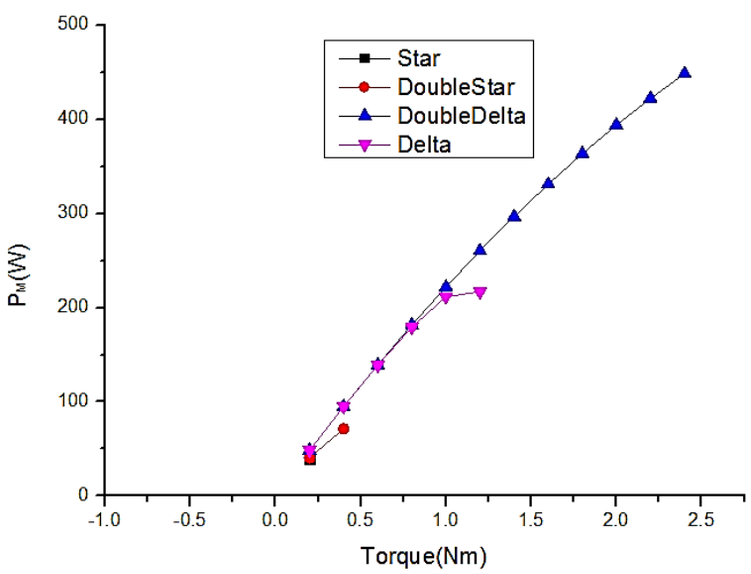

FIGURE 13. Mechanical power in varies connection.

Figure 14 illustrates the current waveform for both star and delta connections. In Figure 14(a), the star connection shows that the current starts at a high value and gradually decreases to a steady state after 5 seconds of operation. After this period, the current stabilizes at a very low level. In contrast, Figure 14(b) shows that in the delta connection, the current remains high throughout the operation but is not stable.

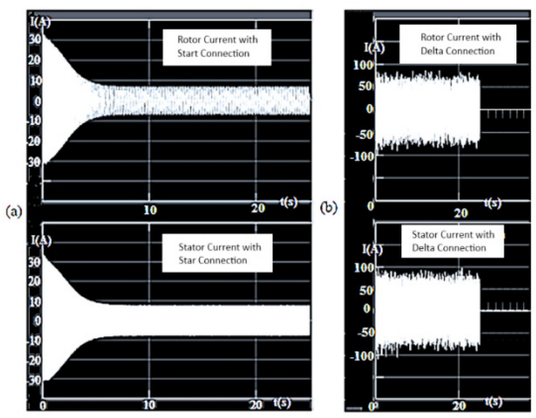

FIGURE 14. Rotor current and stator current (a) Delta connection; (b) Star connection.

CONCLUSION

The effects of the star-delta configuration on the FESS were investigated. The double star-delta configuration in this system not only synchronizes the speed of the FMG but also reduces the system's power consumption. Additionally, using a low-power double motor helps lower development and maintenance costs, whereas a high-power motor would be more expensive. Therefore, this investigation concludes that the double star-delta configuration, combined with PID speed control using frequency, effectively addresses the need for higher torque to drive the high-inertia flywheel while ensuring FMG speed synchronization. Furthermore, it achieves power consumption reduction with lower development and maintenance costs. However, the limitations of FESS are complex control coordination, mechanical stress and wear, high initial cost, thermal management challenges, switching transients and efficiency losses at low load. The study has also mentioned a few potential future works, such as advanced control algorithms, efficiency optimization, dynamic switching strategies, energy management integration, mechanical and thermal design improvements, grid interaction studies.

ACKNOWLEDGEMENT

The authors would like to express their sincere gratitude to Universiti Kebangsaan Malaysia for providing the research facilities and opportunities for their financial support.

DECLARATION OF COMPETING INTEREST

None.

REFERENCES

ALI, M. S., Mahidur, R. S., Ahmad A.I., & Ramizi, M. 2021. A high gain variable boost DC-DC converter for low-voltage hybrid direct methanol fuel cell batteries. *Przeglad Elektrotechniczny* 97 (11): 1–10.

Ali, M.S. 2021. High efficiency flywheel motor generator model with frequency converter controlled. *Przegląd Elektrotechniczny* 1 (11): 186–191.

Anjitha, R S, Rahul, R., Sajay, M. G., Shahabas, N., & Geethu, J. 2017. Soft switch starter for low power three phase induction motor. (03):5–9.

Bekiroglu, E., & Sadullah, E. 2023. Peak shaving control of EV charge station with a flywheel energy storage system in micro grid. *11th International Conference on Smart Grid, IcSmartGrid 2023*.

Bokde, D. M, Jalkote, S.S., Birajdar, M.V., Biradar, R.S. & Jspm B. 2017. Energy conservation using automatic star-delta-star starter. *International Research Journal of Engineering and Technology(IRJET)* 4 (4): 103–106.

Cao, Dongzhi, Liangzhong, Y., Siyang, L., Jian, X., Beilin, M. & Bo, X. 2023. A coordinated control strategy of flywheel-battery hybrid energy storage system for participating in grid frequency regulation. *2023 International Conference on Power Energy Systems and Applications, ICoPESA 2023*, 283–288.

Dwivedi, Anurag, Vishwas, C., Pradnya, C., & Deasi, R.S. 2017. Automatic star delta starter using relay and adjustable electronic timer for 3 phase induction motor. *International Research Journal of Engineering and Technology(IRJET)* 4 (6): 1216–1218.

Ferreira, Fernando, J.T.E., Jose, A., Andre, M. Silva, & Anibal T. D. A. 2020. Saturation-related losses in induction motors for star and delta connection modes. *Proceedings - 2020 International Conference on Electrical Machines, ICEM 2020*, August, 1586–1593.

Garcia, P., Hilel, Marcos, B., Guillermo, M.L., Juan, I. Perez, D., & Jose, I.S. 2022. Comparison and influence of flywheels energy storage system control schemes in the frequency regulation of isolated power systems. *IEEE Access* 10: 37892–37911.

Huang, Chung, N., & Yui, S.C. 2017. Design of magnetic flywheel control for performance improvement of fuel cells used in vehicles. *Energy* (118): 840–852.

Ibrahim, S. 2018. Simulation model for analysis the induction motor starting methods in term of electrical power quality. *International Journal of Scientific & Engineering Research* 9 (7): 816–820.

Itajiba, J.A., Cézar, A.C.V., Sergio, H.L.C, Stéfano F.S., Valderi, R.Q.L., Raúl, G.O., & Kin, C. Y. 2021. Experimental comparison of preferential vs. common delta connections for the star-delta starting of induction motors. *Energies* 14 (5): 1-15.

Koradiya, M.R., Makwana, T.I. & Makwana, N.A., Solanki, A.K. 2019. Control of industrial boiler with temperature controller and motor speed control using AC drive Dr Subhash Technical Campus, India 7 (02): 760–764.

Kusmantoro, Adhi, W. Theodora, I. & Sigit, R. 2017. Soft starter induction motor three phase with fuzzy logic controller inside delta. *International Journal of Applied Engineering Research* 12 (19): 8338–8345.

Mahrouch, A., M. Ouassaid, R. Asghar, M. K. Hasan, & Çakmak, R. 2024. An improved grid-forming control strategy for microgrid stability in modern power system. *IFAC-PapersOnLine* 58 (13): 691–696.

Mohammed, G.M., Dahaman, I., Muhammad, N. H., & Mohamed, S. 2024. Performance comparison and analysis of four- and six-switch inverter controls of BLDC motor employing deep learning. *Jurnal Kejuruteraan* 36 (4): 1409–1422.

Mouratidis, P., Benedikt, S., & Stephan, R. 2019. Hybrid energy storage system consisting of a flywheel and a lithium-ion battery for the provision of primary control reserve. *8th International Conference on Renewable Energy Research and Applications, ICRERA 2019*, November, 94–99.

Murayama, M., Shuhei, K., Hiroaki, T., Shunji, T.I, & Ryuichi, S. 2018. Combination of flywheel energy storage system and boosting modular multilevel cascade converter. *IEEE Transactions on Applied Superconductivity* 28 (3):1-4.

Nemsi, S., Seifeddine, B., Saida, M., & Linda, B. 2018. Parallel operation of flywheel energy storage systems in a microgrid using droop control. *International Conference on Wind Energy and Applications in Algeria, ICWEAA* July.

Pindoriya, R.M., Mishra, A.K. Rajpurohit, B.S. & Kumar, R. 2018. FPGA based digital control technique for BLDC motor drive. *IEEE Power and Energy Society General Meeting* 2018-August (December).

Prasanthi, A., Hussain, S., Madathodika, A., Ahmad, A. I., & Rachid, E. 2021. Optimization of hybrid energy systems and adaptive energy management for hybrid electric vehicles. *Energy Conversion and Management* 243 (September): 114357.

Premkumar, M., & Sowmya, R. 2017. Energy efficient operation of three phase induction motor using delstar converter for machine tools. *International Journal of Electrical and Computer Engineering (IJECE)* 7 (4): 1706–1713.

Ramesh, S.S., Denis, A., Niranjan, K.N., Khalid, H. K., Khalid, G.M., Mayyadah, S.I., & Dinesh, K. 2018. Performance analysis of three-phase induction motor with AC direct and VFD. *IOP Conference Series: Materials Science and Engineering* 331 (1): 012025.

Shubham, S. 2016. Star – Delta starter using static switches with raspberry- PI as a base drive circuit 3 (12): 112.

Salimin, N.N., Sallehuddin, M.H., & Mohd, H.M. S. 2023. Analytical formulation for optimisation of torque density in magnetic gears. *Jurnal Kejuruteraan* si6 (2): 219–228.

Saputra, I.A.D., Suryawan, I.K., & Sugirianta, I. B.K. 2020. Star-delta starting of induction motor stages visualisation using arduino and LabVIEW. *Journal of Physics: Conference Series* 1450 (1): 012037.

Soheli, S.N.,& Saidul, H. 2018. 3 Phase motor by using 3 phase star delta starter voltage reducing method with inverter. *3 Phase Motor by Using 3 Phase Star Delta Starter Voltage Reducing Method with Inverter* 5 (11): 19–22.

Usha, S., Geetha, P. Geetha, A., Palanisamy, R., Thamizh, T.M., Bidyut, M., Nimay, C.G., & Mohammed, A. 2024. Performance enhancement of sensorless induction motor drive using modified direct torque control techniques for traction application. *Alexandria Engineering Journal* 108 (December): 518–538.

Xie, D., Xin, W., Yangtian, N., Sheng, Y., & Zhicheng, Z. 2023. Power system restoration method with the flywheel energy storage support. *2023 8th International Conference on Power and Renewable Energy, ICPRE 2023*, 1028–1032.

Yu, J., Jingyang, F., & Yi, Tang. 2018. Inertia emulation by flywheel energy storage system for improved frequency regulation. *2018 IEEE 4th Southern Power Electronics Conference, SPEC 2018*, July.

Zhao, J., Youzhen, L., Dilong, F., Haodong, R., Liang, Z., & Xiubin, Z. 2023. Capacity optimization of lithium battery-flywheel hybrid energy storage system. *2023 3rd International Conference on Energy Engineering and Power Systems, EEPS 2023*, 186–189.

Zhou, Y., Yanbao, L., Qichao, L., Dongyuan, L., Yuanzhao, Y., & Jianyong, Z. 2020. Investigation of a high speed permanent magnet synchronous machine for magnetic suspended flywheel energy storage system. *2020 IEEE 4th Conference on Energy Internet and Energy System Integration: Connecting the Grids Towards a Low-Carbon High-Efficiency Energy System, EI2 2020*, October, 2733–2737.